Does photodissociation of molecular oxygen from myoglobin and hemoglobin yield singlet oxygen?

ARTICLE *in* JOURNAL OF PHOTOCHEMISTRY AND PHOTOBIOLOGY. B, BIOLOGY · JANUARY 2013

Impact Factor: 2.96 · DOI: 10.1016/j.jphotobiol.2012.12.012 · Source: PubMed

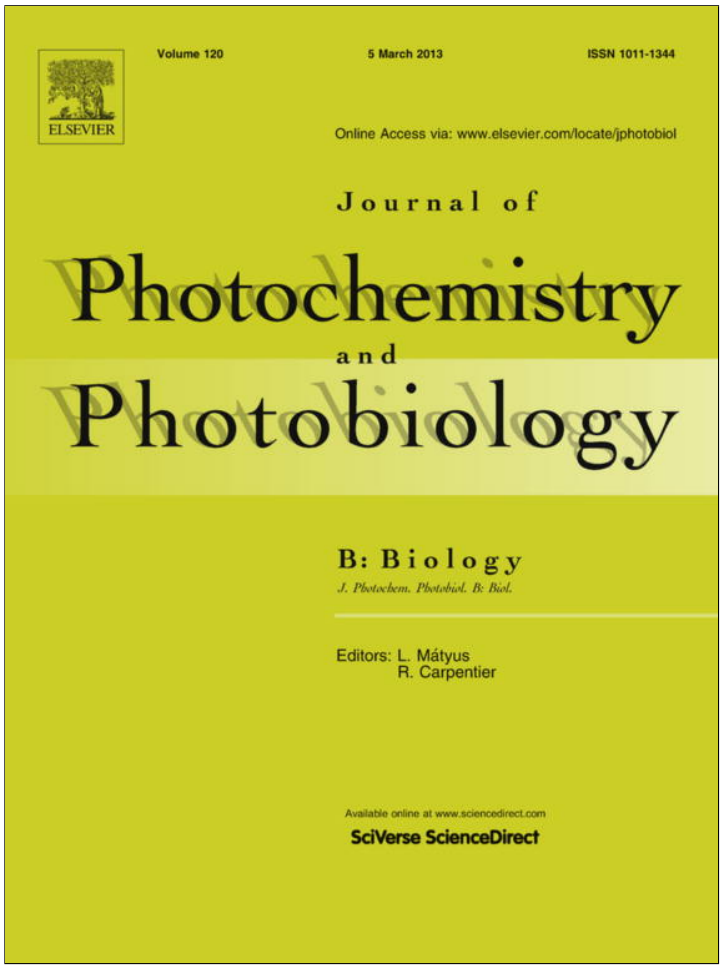

Journal of Photochemistry and Photobiology B: Biology 120 (2013) 130–141

Contents lists available at SciVerse ScienceDirect

Journal of Photochemistry and Photobiology B: Biology

journal homepage: www.elsevier.com/locate/jphotobiol

Does photodissociation of molecular oxygen from myoglobin and hemoglobin yield singlet oxygen?

Sergei V. Lepeshkevich *, Alexander S. Stasheuski, Marina V. Parkhats, Victor A. Galievsky, Boris M. Dzhagarov

B.I. Stepanov Institute of Physics, National Academy of Sciences of Belarus, 68 Nezavisimosti Ave, Minsk 220072, Belarus

ARTICLE INFO

Article history:
Received 21 September 2012
Received in revised form 20 December 2012
Accepted 30 December 2012
Available online 7 January 2013

Keywords:
Singlet oxygen
Myoglobin
Hemoglobin
Photodissociation
Luminescence
Quantum yield

ABSTRACT

Time-resolved luminescence measurements in the near-infrared region indicate that photodissociation of molecular oxygen from myoglobin and hemoglobin does not produce detectable quantities of singlet oxygen. A simple and highly sensitive method of luminescence quantification is developed and used to determine the upper limit for the quantum yield of singlet oxygen production. The proposed method was preliminarily evaluated using model data sets and confirmed with experimental data for aqueous solutions of 5,10,15,20-tetrakis(4-*N*-methylpyridyl) porphyrin. A general procedure for error estimation is suggested. The method is shown to provide a determination of the integral luminescence intensity in a wide range of values even for kinetics with extremely low signal-to-noise ratio. The present experimental data do not deny the possibility of singlet oxygen generation during the photodissociation of molecular oxygen from myoglobin and hemoglobin. However, the photodissociation is not efficient to yield singlet oxygen escaped from the proteins into the surrounding medium. The upper limits for the quantum yields of singlet oxygen production in the surrounding medium after the photodissociation for oxyhemoglobin and oxymyoglobin do not exceed 3.4×10^{-3} and 2.3×10^{-3}, respectively. On the average, no more than one molecule of singlet oxygen from every hundred photodissociated oxygen molecules can succeed in escaping from the protein matrix.

1. Introduction

Molecular oxygen (O_2) is one of the most important molecules on Earth. The majority of living organisms utilize O_2 for respiration [1]. Singlet oxygen ($O_2(^1\Delta_g)$ or $^1O_2$), the lowest excited electronic state of O_2, is a highly reactive species playing a significant role in chemical and biological systems [2–6]. The most common method of $^1O_2$ generation is photosensitization wherein the energy of a sensitizer excited state, which is formed by an absorption of light, is transferred to the electronic ground state of molecular oxygen ($^3\Sigma_g^-$) [2,4,7]. For the most organic sensitizers, the relevant excited state is the lowest triplet. Many protein-bound chromophores like chlorophyll in the isolated reaction center of Photosystem II can generate singlet oxygen [8]. Singlet oxygen is also produced by enzymatic and chemical reactions. Unequivocal evidence for the $^1O_2$ generation in enzymatic reactions has been obtained in a number of peroxidase [9,10], dioxygenase [11], and methemoglobin systems [12]. Singlet oxygen appears to be a key component in oxidation reactions of host defense and immune system [13,14]. Today it is well-known that $^1O_2$ mediates both apoptotic and necrotic pathways of cell death induced by photodynamic therapy [15]. This explains a strong interest in a direct observation of the generation and quenching of $^1O_2$ in biological objects.

One of the most simple biological reactions involving molecular oxygen is the binding of O_2 to myoglobin and hemoglobin, i.e. the binding of O_2 to the Fe(II) ion in a heme group. It has been shown experimentally [16] that the deoxyheme has a high-spin quintet ground state. The nonbound molecular oxygen has a triplet ground state ($^3\Sigma_g^-$). Therefore, there are six unpaired electrons per these two molecules. Upon the binding, the unpaired spins on the deoxyheme and O_2 are expected to be either parallel, giving rise to a septet, or antiparallel, giving rise to a triplet state. However, experimentally, the oxygenated heme has a singlet ground state. Therefore, this is a spin-crossing reaction. The literature is rich in discussions about the nature of the Fe–O_2 bond [16–21]. Pauling [21] suggested that the electronic structure of oxyheme is better described as the ferrous low spin iron bound to the oxygen molecule, residing in a spin-paired singlet configuration analogous to that in the $^1\Delta_g$ molecular state. Goddard and Olafson [19] proposed that both the iron and oxygen are in triplet states. On the other hand, Weiss [20] pointed out that the low-spin ferric ion and superoxide anion are antiferromagnetically coupled. Theoretical

* Corresponding author. Tel.: +375 17 284 0795; fax: +375 17 284 0879.
E-mail address: lepeshkevich@imaph.bas-net.by (S.V. Lepeshkevich).

1011-1344/$ - see front matter © 2013 Elsevier B.V. All rights reserved.
http://dx.doi.org/10.1016/j.jphotobiol.2012.12.012

calculations [16,17] suggested that the FeO_2 core could be considered as a practically equal mixture of Pauling [21] and Weiss pictures [20]. This is in accordance with the experimental observation that a quantum mixture of approximately two-thirds ferric and one-third ferrous states gives the best agreement with Mössbauer spectra [22]. Therefore, the oxyheme is inherently multiconfigurational. Thus, photodissociation of the oxyheme is expected to result in the generation of the deoxyheme in a singlet state plus the highly reactive singlet oxygen.

The aim of the present study is to investigate whether $^1O_2$ can be generated during the photodissociation of molecular oxygen from myoglobin and hemoglobin. It is found that oxymyoglobin and oxyhemoglobin irradiation with visible light does not produce any detectable amount of singlet oxygen. A simple and highly sensitive method of luminescence quantification is reported and used to determine the upper limit for the quantum yield of $^1O_2$ production. The theory of the proposed method is presented in a general form. Then, a comprehensive evaluation is carried out on model data sets whose signal-to-noise ratio is smoothly varied. A confirmation of the method on experimental data is reported as well.

2. Experimental section

2.1. Materials

The tosylate salt of 5,10,15,20-tetrakis(4-*N*-methylpyridyl) porphyrin, TMPyP, was a generous gift from Dr. V.L. Malinovsky.

Oxygenated human hemoglobin was purified according to a previously described protocol [23]. Horse heart metmyoglobin (Sigma) was of the highest purity available and was used as received. Concentrated purified native myoglobin in a buffer was fully reduced by addition of sodium dithionite. The solution was mixed gently and immediately gelfiltered on a Sephadex G-25 (Pharmacia) column equilibrated with the O_2-saturated buffer to separate excess dithionite and allow myoglobin oxygenation. Fractions containing oxymyoglobin were collected.

All experiments were carried out at 20 °C in 25 mM Tris–HCl buffer, pH 7.4. Concentrations were determined spectrophotometrically. Protein concentrations were 50 μM on a per heme basis. All measurements were carried out in 10 mm × 10 mm quartz cuvettes in air-saturated solutions.

2.2. Time-resolved singlet oxygen detection

Time-resolved luminescence in the near-infrared region (NIR) was measured on a nanosecond laser NIR spectrometer designed and developed in our laboratory. The present setup is a modified version of a previously described one [24]. Samples were excited by the second harmonic (532 nm) of an Nd:YAG laser (DTL-314QT, Laser-export Co. Ltd.). Typical parameters of the laser were as follows: the pulse width of 10 ns, the pulse energy of 0.4 μJ, and the repetition rate of 1 kHz. Luminescence radiation was collected with a high-throughput optical system, spectrally isolated with bandpass filters (less than 13 nm FWHM) (Thorlabs GmbH; Axicon) and directed to a photomultiplier tube, PMT (model H10330A-45, Hamamatsu Photonics K.K.), with a InP/InGaAsP photocathode cooled to −60 °C and having a quantum efficiency of ~2% in the spectral range from 950 to 1400 nm. After amplification by 1.6 GHz HFAC-26 unit (Becker & Hickl GmbH), the output of the PMT was sent to a multiscaler photon counter (P7888-2, FAST ComTec GmbH). The multichannel scaling technique was used to detect all output PMT pulses with a count rate close to the capability of the detector. The multiscaler enables to count signals with a time resolution of 1 ns. To minimize samples photodegradation, continuous magnetic stirring was used.

2.3. Luminescence emitted by photosensitized singlet oxygen

The direct detection of $^1O_2$ generated during the photodissociation of molecular oxygen from the proteins was performed by measuring $^1O_2$ luminescence at 1270 nm. To quantify the $^1O_2$ generation, the estimated intensity of $^1O_2$ luminescence was compared with the one emitted by $^1O_2$ generated by a known standard, namely the highly effective water-soluble cationic photosensitizer TMPyP [25,26] (for further details of the comparison, see Sections 4, 4.2–4.5). The experimentally measured time-dependent intensity for the standard, $S_{st}(t)$, as well as for any photosensitizer, is proportional to the photosensitized $^1O_2$ concentration, $[^1O_2^{st}](t)$:

$$S_{st}(t) = \frac{\kappa}{n^2} k_r^s [^1O_2^{st}](t), \tag{1}$$

where κ is a proportionality constant that contains geometrical and electronic factors of the detection system, n is the refractive index of solvent, and k_r^s is the rate constant of solvent-dependent $^1O_2$ radiative decay [27]. In their turn, the time dependence of photosensitized $^1O_2$ concentration is given by:

$$[^1O_2^{st}](t) = \frac{k_{T_1\Delta}[O_2][T_1]_{t=0}}{k_T - k_\Delta}(e^{-k_\Delta t} - e^{-k_T t}), \tag{2}$$

where $k_{T_1\Delta}$ is the rate constant of energy transfer between the excited triplet state of sensitizer and the ground-state molecular oxygen, resulting in the $^1O_2$ production. $[O_2]$ is the concentration of O_2 in solvent. $[T_1]_{t=0}$ is the initial concentration of the sensitizer triplet state T_1. k_T is the rate constant of sensitizer triplet state deactivation; k_Δ is the rate constant of $^1O_2$ deactivation in water. Symbols used frequently in this paper are summarized in Table 1. Eq. (2) is true in the case of a homogeneous environment, low laser energy, delta pulse excitation, and when there is no back transfer of energy from singlet oxygen to the photosensitizer triplet state [28]. All these conditions are fulfilled for experiments with the standard.

2.4. Kinetic method of luminescence quantification

Within the framework of the kinetic model, the time-dependent luminescence intensity is generally described by a function $S(t,p_1, \ldots, p_m)$ with a finite number of parameters, $p_j (j = \overline{1,m})$. Hence, the integral intensity of luminescence, I, can be represented in a functional form as:

$$I = \int_0^\infty S(t, p_1, \ldots, p_m)dt = F(p_1, \ldots, p_m). \tag{3}$$

The present parameters, $p_j (j = \overline{1,m})$, are found by nonlinear weighted least-squares fitting of the chosen model function $S(t,p_1, \ldots, p_m)$ to the data. The mean values and 95% confidence intervals for the parameters, $\langle p_j \rangle$ and $\Delta p_j (j = \overline{1,m})$, respectively, are obtained from independently repeated experiments. Subsequently, the mean value of the integral intensity, $\langle I \rangle$, and its 95% confidence interval, ΔI, are calculated as: $\langle I \rangle = F(\langle p_1 \rangle, \ldots, \langle p_m \rangle)$ and $\Delta I = \left(\sum_{j=1}^m \left(\frac{\partial F}{\partial p_j} \right)^2 \Delta p_j^2 \right)^{1/2}$, respectively. In the last equation, the partial derivatives are evaluated at the mean values of the parameters.

Taking into account Eqs. (1)–(3), one can obtain the integral intensity of luminescence emitted by photosensitized $^1O_2$:

$$I_{st} = \frac{\kappa}{n^2} \frac{k_r^s k_{T_1\Delta}[O_2][T_1]_{t=0}}{k_\Delta k_T}. \tag{4}$$

The number of $^1O_2$ molecules formed per absorbed photon by a sensitizer defines the quantum yield of photosensitized $^1O_2$ generation, Q_Δ^{st}. The quantum yield of $^1O_2$ generation by the chosen standard, Q_Δ^{st}, is known to be equal to 0.77 ± 0.04 [26]. The quantum yield Q_Δ^{st} is determined by two factors:

Table 1
List of frequently used symbols.

k_r^s	Rate constant of solvent-dependent $^1O_2$ radiative decay
k_{nr}^s	Rate constant of solvent-dependent $^1O_2$ nonradiative decay
k_T	Rate constant of sensitizer triplet state deactivation
k_r^p	Rate constant of protein-dependent $^1O_2$ radiative decay
k_{nr}^p	Rate constant of protein-dependent $^1O_2$ nonradiative decay
$k_{T_1\Delta}$	Rate constant of energy transfer between the excited triplet state of sensitizer and the ground-state molecular oxygen, resulting in the $^1O_2$ production
k_Δ^p	Rate constant of $^1O_2$ deactivation within proteins
k_Δ	Rate constant of $^1O_2$ deactivation in water
k_{gem}	Rate constant for the geminate $^1O_2$ rebinding to the heme iron
k_{out}	Rate constant for $^1O_2$ escape from the protein
k_{in}	Rate constant for $^1O_2$ entry into proteins
Q_T	Quantum yield of sensitizer triplet state formation
Q_Δ^{st}	Quantum yield of photosensitized $^1O_2$ generation by the standard
Q_Δ^s	Quantum yield of $^1O_2$ production in the surrounding medium after the photodissociation
Q_Δ^p	Primary quantum yield of $^1O_2$ production after the photodissociation
$[^1O_2^s]_{t_{max}}$	Maximal concentration of $^1O_2$ in the surrounding medium after the photodissociation
S	Intensity of luminescence
$[T_1]_{t=0}$	Initial concentration of the sensitizer triplet state T_1
$[^1O_2^p]_{t=0}$	Initial concentration of $^1O_2$ within proteins after the photodissociation
f_Δ	Fraction of sensitizer triplets deactivated by molecular oxygen with $^1O_2$ production
$[P]$	Concentration of proteins in solvent
$[^1O_2^{st}]$	Concentration of photosensitized $^1O_2$
$[O_2]$	Concentration of O_2 in solvent
$[^1O_2^p]$	Concentration of $^1O_2$ within proteins after the photodissociation
$[^1O_2^s]$	Concentration of $^1O_2$ in the surrounding medium after the photodissociation
δ	Efficiency of $^1O_2$ escape from the protein matrix
β	Absorption factor
I	Integral intensity of luminescence
n	Refractive index
N	Number of moles of photons striking upon a working volume V
t_{max}	Time when the concentration of $^1O_2$ in the surrounding medium reaches its maximal value after the photodissociation
V	Working volume
κ	Proportionality constant that contains geometrical and electronic factors of the detection system

$$Q_\Delta^{st} = Q_T f_\Delta, \tag{5}$$

Here, Q_T is the triplet quantum yield, defined as the amount of sensitizers in the photoexcited triplet state relative to the amount of originally excited chromophores:

$$Q_T = \frac{[T_1]_{t=0}}{(N/V)\beta_{st}}, \tag{6}$$

where N is the number of moles of photons striking upon a working volume V. β_{st} is the sensitizer absorption factor determined by $\beta_{st} = 1 - 10^{-A_{st}}$, where A_{st} is the sensitizer absorbance at the excitation wavelength. The second factor in Eq. (5), f_Δ, is the fraction of triplets deactivated by molecular oxygen with $^1O_2$ production:

$$f_\Delta = \frac{k_{T_1\Delta}[O_2]}{k_T}. \tag{7}$$

As a result, using Eqs. (4)–(7), the integral intensity I_{st} can be expressed in terms of the quantum yield Q_Δ^{st}:

$$I_{st} = Q_\Delta^{st}\frac{\kappa}{n^2}\frac{k_r^s}{k_\Delta}(N/V)\beta_{st} \tag{8}$$

2.5. Proposed method of luminescence quantification (theoretical background)

Ideally, when in kinetic traces, the signal $S(t)$ is only present, i.e. noise and background are absent, the integral intensity I can be calculated using the formula:

$$I = \lim_{\Delta t_i \to 0}\sum_{i=1}^{n} S(t_i)\Delta t_i. \tag{9}$$

Here, Δt_i is the integration time step (time bin), $\Delta t_i = t_{i+1} - t_i$, $1 \leqslant i \leqslant n$; n is the number of time steps $[t_i, t_{i+1}]$. The signal $S(t)$ is restricted to a closed interval $[t_1, t_{n+1}]$. If the amplitude of the signal $S(t)$ is quantized, then Eq. (9) can be represented as:

$$I = \lim_{\Delta t_i \to 0}\sum_{i=1}^{n} N_i\Delta t_i, \tag{10}$$

where N_i is the sum of quanta (counts) at the time bin Δt_i. If the time bin is constant and equal to Δt, then Eq. (10) reduces to the following:

$$I = N_S\Delta t, \tag{11}$$

where N_S is the overall number of counts in the kinetics. In the general case, when both background and noise are present in the kinetics, Eq. (11) should be modified as follows:

$$I = (N_S - N_N)\Delta t, \tag{12}$$

where N_N is the overall number of noise and background counts. At first glance it would seem that the value N_N can be directly determined in an additional experiment, where only noise and background are measured in the absence of signal. However, it is difficult to realize because noise distributions, obtained in independent experiments, can differ sufficiently. Hence, noise and background features should be directly retrieved from the experimental kinetics containing the signal component. For this purpose, let's assume that the time window of the signal $S(t)$ is known *a priori*, i.e. the moment, when the signal disappears practically completely after the photoexcitation, is known. Hence, each kinetics can be measured in a specially chosen time interval, which can be divided into two sequential parts containing an equal considerable number of time bins so that (i) the signal $S(t)$ has nonzero values only in the first part of the time interval and (ii) the noise and background in the former and latter parts of the kinetics are the same. Within the framework of these assumptions, in Eq. (12), N_S can be

considered as the overall number of counts in the former part of the kinetics, and N_N – the overall number of counts in the latter part. To confirm the accuracy of the proposed method, model and experimental data sets are analyzed in the next two sections. Additionally, the proposed method is compared with the kinetic one. For this purpose, uncertainties in all values obtained by both methods are presented as 95% confidence intervals.

3. Results

3.1. Test Case I: model kinetics

Model kinetics were generated by utilizing the following equation, being the compact form of Eqs. (1) and (2):

$$S(t) = \frac{a}{k_T - k_\Delta}(e^{-k_\Delta t} - e^{-k_T t}) \quad (13)$$

where a is a constant. Here, the rate constants k_Δ and k_T were kept constant and equal to $2.8 \times 10^5\ s^{-1}$ and $5 \times 10^5\ s^{-1}$, respectively, being typical for $^1O_2$ luminescence in water [29–32]. Eight different nonzero constants a were arbitrary taken, being varied over 3 orders of magnitude, from 0.16 to $320\ s^{-2}$. A constant background $b = 7.8 \times 10^5\ s^{-1}$ as well as a Gaussian noise with a time-independent standard deviation of $\sigma = 320\ s^{-1}$ were added to each generated signal $S(t)$. The abovementioned parameters were intentionally chosen to receive noisy kinetics. Three kinetics with the smallest nonzero signal-to-noise ratios are shown in Fig. 1*A* (a_1, a_2, and a_3). The noise generation was repeated five times, i.e. five trials were performed. Subsequently, for each signal $S(t)$ with the constant a, five model kinetic traces were obtained. Additionally, five ones containing only the background and random noise were generated (see, for example, Fig. 1A (a_0)). As a result, 45 model kinetics were obtained. Subsequently, all these kinetic traces were independently analyzed by the proposed and kinetic methods. The results of the proposed analysis are shown in Fig. 1B (*symbols*). The integral intensity I on the ordinate is plotted versus the trial number on the abscissa. The dashed lines show the expected integral intensities I calculated from the relationship

$$I = \frac{a}{k_T k_\Delta}, \quad (14)$$

with the given values of a, k_T, and k_Δ. The amplitudes a are indicated near the corresponding lines. As it is seen, the integral intensities I obtained by the proposed method coincide with the expected ones. A good coincidence of the expected integral intensities with the ones calculated by the kinetic method is also observed (not shown). For the integral intensity determination by the kinetic method, the expected parameters of Eq. (13) were taken as an initial estimate for the fit. The Levenberg–Marquardt fitting algorithm was used. At given a, the final integral intensity and its relative error were obtained from the average over all the independent trials. The relative errors of integral intensity determined by the proposed (*circles*) as well as kinetic method (*triangles*) are shown in Fig. 1C. As it is seen, the relative errors estimated by these methods differ by an order of magnitude, the proposed method being more accurate than the kinetic one. The difference in the relative errors estimated by two methods decreases at a signal-to-noise ratio improvement. However, the ratio of the relative errors remains practically constant.

3.2. Test Case II: experimental kinetics

Time-resolved $^1O_2$ luminescence traces, generated by photoexcitation of photosensitizer TMPyP, were used as experimental kinetics. The light emission at 1270 nm corresponding to $^1O_2$ monomolecular decay ($^1\Delta_g \rightarrow {}^3\Sigma_g^-$) was monitored. The $^1O_2$ generation was confirmed by spectral analysis of the light emission

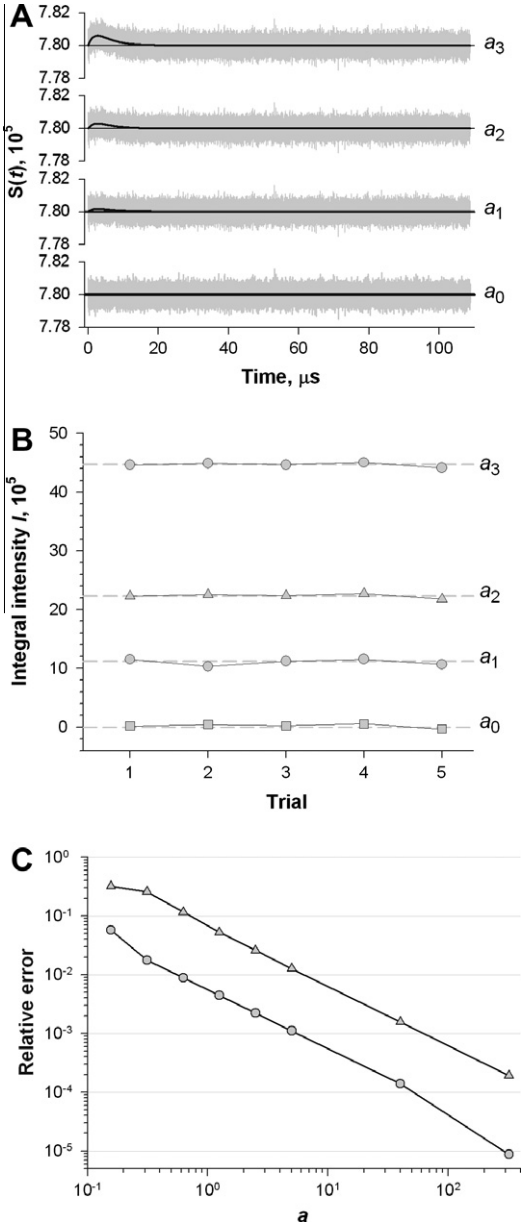

Fig. 1. Test of the proposed method using model kinetics and a comparison between two methods. (A) The model kinetics generated at 108.8 thousand points, the interval between successive time points being $\Delta t = 1$ ns. The following constants were arbitrary taken: $a_0 = 0\ s^{-2}$, $a_1 = 0.16\ s^{-2}$, $a_2 = 0.32\ s^{-2}$, and $a_3 = 0.62\ s^{-2}$. A constant background $b = 7.8 \times 10^5\ s^{-1}$ as well as a Gaussian noise with a time-independent standard deviation of $\sigma = 320\ s^{-1}$ were added to each generated signal. The kinetic traces in the absence and presence of the noise are shown in *black* and *gray*, respectively. (B) The integral intensity I obtained by the proposed method. The integral intensity I on the ordinate is plotted versus the trial number on the abscissa. For each trial, the noise was independently generated. The calculated intensities I are represented by *symbols*. The *dashed lines* show the expected integral intensities calculated according to Eq. (14) at the given values of a, k_Δ and k_T. The constants a are indicated near the corresponding lines. (C) The accuracy of the integral intensity estimated by the proposed and kinetic methods. A comparison of the proposed and kinetic methods by model data testing. *Ordinate*, the relative error in the integral intensity determined by the proposed (*circles*) and kinetic methods (*triangles*). *Abscissa*, the constant a describing the model kinetics (Eq. (13)).

(Fig. 2) and by the quenching effect of sodium azide (not shown). In Fig. 2, the spike-like peak at the beginning of the kinetic traces is due to the scattered laser light and photosensitizer fluorescence. At 1270 nm, the spike is followed by a prominent increase and then a decrease of $^1O_2$ emission. It is important to note that the $^1O_2$ signal is temporally displaced relative to the spike and the latter

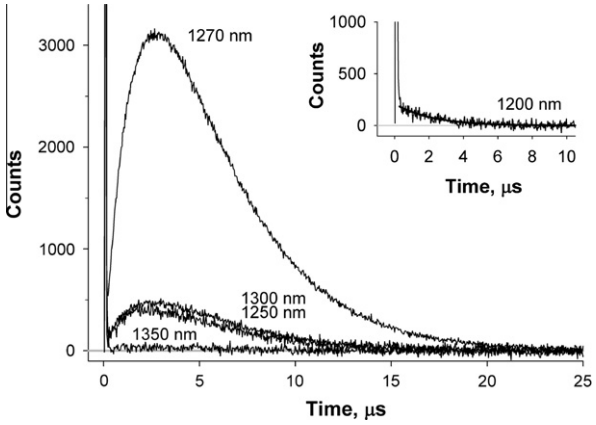

Fig. 2. Time-resolved near-infrared emission traces recorded upon 532 nm irradiation of an air-saturated aqueous solution containing 60 μM TMPyP. The 32 ns time channel width was used on the photon counter. For each of the kinetic trace, data were accumulated for 20 min. The average noise level was subtracted from the kinetics. The spike that precedes the signal assigned to singlet oxygen is due to the scattered laser light and photosensitizer fluorescence. The $^1O_2$ signal is temporally displaced relative to the spike and the latter does not significantly contribute to the observed data of the $^1O_2$ emission at times longer than 570 ns after the laser flash. The time-resolved emission data obtained at 1270 nm were fitted using Eq. (13). Respective rate constants k_Δ and k_T were found to be equal to $(2.78 \pm 0.15) \times 10^5\ s^{-1}$ and $(5.0 \pm 0.5) \times 10^5\ s^{-1}$. The absolute errors for determined rate constants are mainly caused by sample variance. To assign the processes, an additional flash photolysis experiment (setup as in the work [51]) was carried out. The photosensitizer triplet lifetime was determined directly. The faster emission process was assigned to the triplet decay, the slower one to the $^1O_2$ decay. The rate constants measured by us agree well with those reported previously [4,26,29–31]. The emission signal at 1200 nm (*Insert*) decays exponentially with the rate constant equaled to the one for the photosensitizer triplet state deactivation, k_T. Given that the extremely weak signals were detected in the present experiments, the quantum yield of $^1O_2$ luminescence being 6.5×10^{-7} [4], the emission at 1200 nm (*Insert*) can be assigned to photosensitizer phosphorescence or delayed fluorescence.

does not significantly contribute to the observed data of the $^1O_2$ emission at times longer than 570 ns after the laser flash. Therefore, to test the proposed method, the experimental kinetics of time-resolved $^1O_2$ luminescence were analyzed in the time window from 570 ns to 131 μs. Here, each kinetic trace was divided into two equal sequential intervals [570 ns, ~65.8 μs] and [~65.8 μs, 131 μs], each one containing a substantial number of time bins (more than 32.5 thousand). Moreover, the $^1O_2$ luminescence can be considered to have nonzero intensity only in the first time interval.

The experimental kinetics were detected at five following concentrations of TMPyP: 0.09 μM (c_1), 0.26 μM (c_2), 1.0 μM (c_3), 2.8 μM (c_4), and 9.6 μM (c_5). Typical kinetics are shown in Fig. 3A. At each chosen TMPyP concentration, the detection of $^1O_2$ luminescence was repeated five times. As a result, 25 experimental kinetics were obtained. Each kinetic trace was independently subjected to the proposed and kinetic analysis. The results of the proposed analysis are shown in Fig. 3B. At given TMPyP concentration, the final integral intensity and its relative error were obtained from the average over all the independent experiments. Additionally, the relative integral intensities, I/I_{st}, were calculated on the basis of the average values, the most concentrated sample being used as a reference standard, I_{st}. As it is followed from Eq. (8), the integral intensity I_{st} is proportional to the absorption factor β_{st}. Therefore, at a certain dilution of the sample, a change in the normalized absorption factor, β/β_{st}, is expected to be equal to the corresponding change in the relative integral intensity, I/I_{st}. In Fig. 3C (*circles*), the relative integral intensities, I/I_{st}, obtained with the use of the proposed method are plotted versus the normalized absorption factor β/β_{st}. The expected dependence is shown as *a straight line*. As it is seen, the relative integral intensities obtained by the proposed method coincide with the expected ones. A good coincidence of the expected relative integral intensities with the ones calculated by the kinetic method is also observed (not shown). Additionally, in Fig. 3D, the relative errors of relative integral intensities determined by the proposed (*circles*) as well as kinetic method (*triangles*) are shown. As it is seen, the proposed method is more accurate than the kinetic one. For the data with the smallest normalized absorption factor β/β_{st}, the noise is too severe to allow the relative integral intensity determination by the kinetic method. On the other hand, the proposed method provides the integral intensity determination even for the kinetics with extremely low signal-to-noise ratio. Therefore, the proposed method is proven to be a more precise one in comparison with the classical kinetic method. Reducing the number of resulting parameters from three (a, k_T, and k_Δ in the kinetic method) to one (I in the proposed method) allows to increase the accuracy in determining the integral intensity by an order of magnitude. In other words, the loss of kinetic information by the proposed method is compensated by an increase in sensitivity of the integral intensity determination.

3.3. Near-infrared luminescence of oxymyoglobin and oxyhemoglobin

Irradiation of the oxygenated proteins with visible light (532 nm) was used to produce any detectable amount of singlet oxygen at the photodissociation of molecular oxygen from the proteins. Typical kinetics of time-resolved luminescence of oxymyoglobin in the near-infrared region is shown in Fig. 4. As it is seen, only a spike-like peak at the beginning of the kinetic trace is observed, being probably due to the scattered laser light and expected $^1O_2$ emission. To discriminate between these two components, the time-resolved measurements were performed at the following wavelengths: 1200, 1250, 1270, 1300, and 1350 nm. At each wavelength, the measurement was repeated five times. All the kinetic traces were subjected to the proposed analysis. Each kinetics was analyzed independently in two time windows: (1) from −70 ns to 131 μs, containing the whole kinetics with the spike and (2) from 80 ns to 131 μs, without the spike. In every case, the kinetic trace was divided into two equal sequential intervals. At each wavelength, the overall integral intensities I_{total} and their errors ΔI_{total} were obtained from the average over all the independent experiments. As a result, for the kinetic with and without the spike, two spectra were obtained (Fig. 5, *open* and *closed circles*, respectively). As it is seen, there is no characteristic peak of $^1O_2$ emission at 1270 nm. The same measurements for oxyhemoglobin resulted in a similar featureless spectrum (data not shown). To describe the intensity of scattered light, $I_{scatter}$, the calculated data for all but one wavelength (1270 nm) were fitted by a linear function. In Fig. 5, *solid lines* show data fit. The difference between the overall integral intensity, I_{total}, and the intensity of scattered light, $I_{scatter}$, at 1270 nm represents the integral intensity of $^1O_2$ emission, I. The error for I was determined as

$$\Delta I = \sqrt{\Delta I_{total}^2 + \Delta I_{scatter}^2}, \tag{15}$$

where ΔI_{total} is the error for the overall integral intensity I_{total} at 1270 nm, $\Delta I_{scatter}$ is the error for the scattered light intensity, determined as the root mean-square deviation between the linear function describing the scattered light and the overall integral intensities at all but one wavelength (1270 nm). The calculated integral intensities of $^1O_2$ emission, I, are listed in Table 2. As it is seen, in all cases, the mean values $\langle I \rangle$ are smaller than their errors ΔI. Consequently, within the experimental accuracy, the photodissociation of molecular oxygen from myoglobin and hemoglobin does not yield singlet oxygen. However, the calculated errors ΔI (Table 2) can be considered as the upper limits for the integral intensities of $^1O_2$ emission, I, generated by the photoexcitation of the oxygenated proteins.

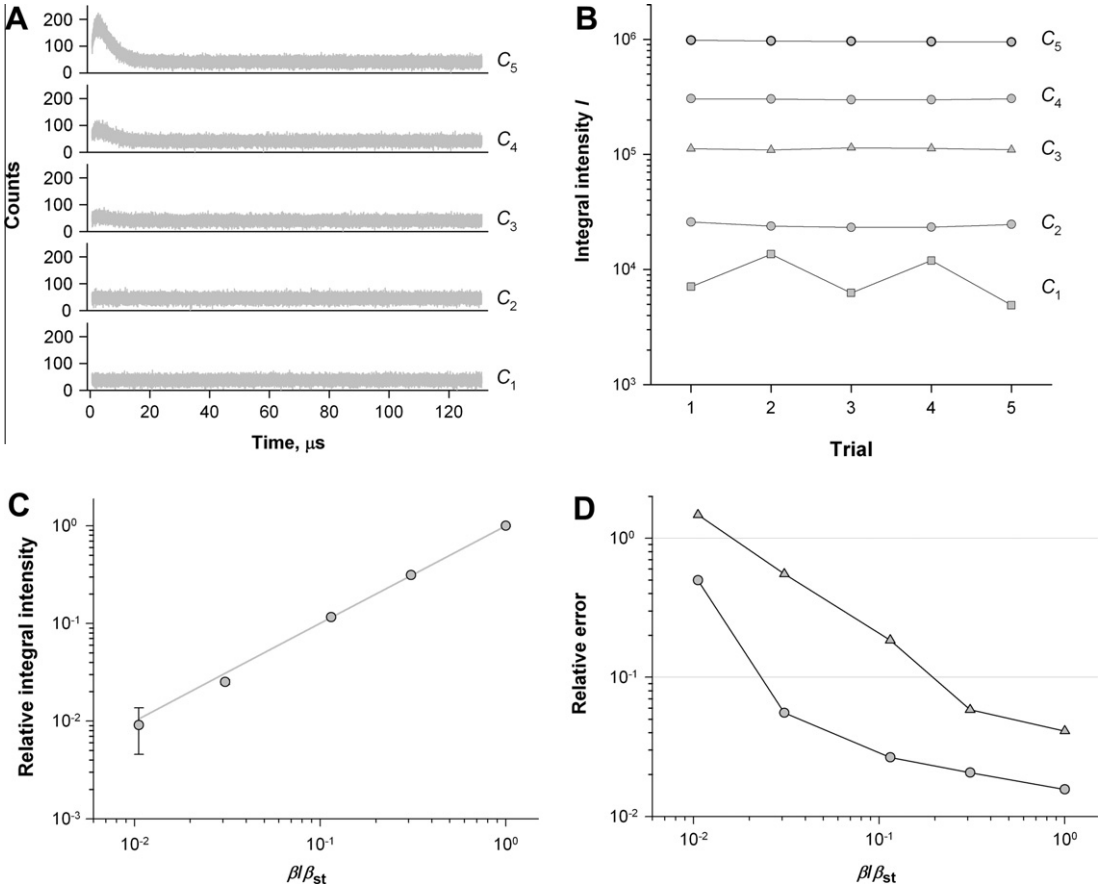

Fig. 3. Test of the proposed method using experimental kinetics and a comparison between two methods. (A) The time-resolved $^1O_2$ luminescence of an air-saturated aqueous solution containing TMPyP. The channel width was 2 ns with a total of ~65.5 thousand channels. The measurement and collection time was 4 min. Detection wavelength, 1270 nm. TMPyP concentration, 0.09 μM (c_1), 0.26 μM (c_2), 1.0 μM (c_3), 2.8 μM (c_4), and 9.6 μM (c_5). (B) The integral intensity I obtained by the proposed method. The integral intensity I on the ordinate is plotted versus the trial number of the abscissa. The calculated intensities are represented by symbols. The TMPyP concentrations C are indicated near the corresponding symbols. (C) A comparison of the expected and calculated relative integral intensities. *Ordinate*, the relative integral intensity I/I_{st}. *Abscissa*, the normalized absorption factor β/β_{st}. The relative integral intensities I/I_{st} calculated by the proposed method are represented by *circles*, the expected ones are shown as a *straight line*. (D) A comparison of the proposed and kinetic methods by experimental data testing. The accuracy of the relative integral intensity estimation by the proposed and kinetic methods. *Ordinate*, the relative error in the relative integral intensity determined by the proposed (*circles*) and kinetic methods (*triangles*). *Abscissa*, the normalized absorption factor.

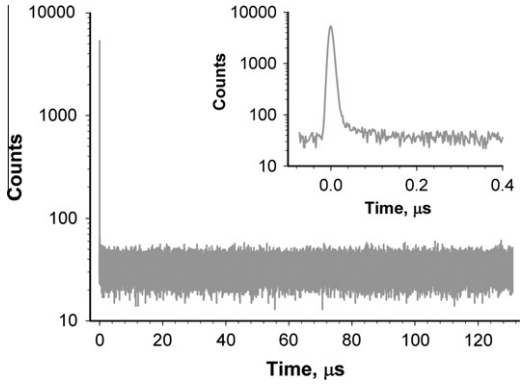

Fig. 4. Time-resolved luminescence of oxymyoglobin in the near-infrared region. The channel width was 2 ns with a total of ~65.5 thousand channels. The measurement and collection time was 4 min. Detection wavelength, 1270 nm. Myoglobin concentration, 50 μM.

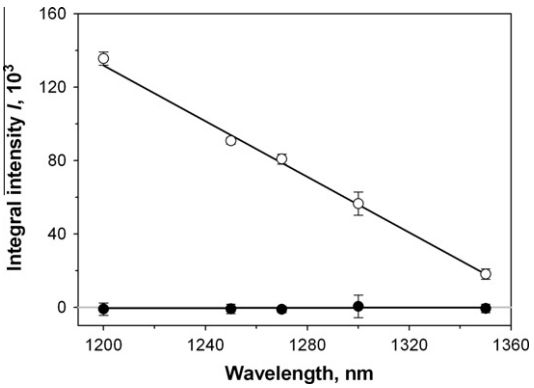

Fig. 5. Spectra obtained by the proposed analysis of the time-resolved luminescence of oxymyoglobin. The calculated overall integral intensities I_{total} with confidence intervals ΔI_{total} are represented by circles and error bars, respectively. In some cases the confidence interval bars do not extend beyond the size of the symbols. *Open* and *closed circles* represent the results of independent analyses in two time windows: (1) from −70 ns to 131 μs and (2) from 80 ns to 131 μs, respectively. *Solid lines* represent fit of the calculated data for all but one wavelength (1270 nm) to a simple linear function. Myoglobin concentration, 50 μM.

4. Discussion

4.1. Photodissociation of singlet oxygen from myoglobin and hemoglobin

Photodissociation of liganded myoglobin and hemoglobins is a well-known phenomenon (see, for example, the works [33,34] and references herein). This process has been extensively used to investigate ligand rebinding kinetics and protein relaxation dynamics [34–37]. With the advent of lasers generating ultrashort

Table 2
The integral intensity of $^1O_2$ luminescence, I, for oxymyoglobin (MbO_2) and oxyhemoglobin (HbO_2).

Protein	Time window[a]	I [b] ($\times 10^3$)	I_{st} [c] ($\times 10^6$)	β_{st}/β
MbO_2	[−70 ns, 131 μs]	2.0 ± 3.9	1.45 ± 0.02	1.46
MbO_2	[80 ns, 131 μs]	−0.8 ± 1.9	1.45 ± 0.02	1.46
HbO_2	[−70 ns, 131 μs]	2.5 ± 9.1	1.46 ± 0.05	0.96
HbO_2	[80 ns, 131 μs]	−0.6 ± 3.7	1.46 ± 0.05	0.96

The channel width was 2 ns with a total of ~65.5 thousand channels. Protein concentrations, 50 μM on a per heme basis. TMPyP concentration, 60 μM.
The uncertainties are presented as 95% confidence intervals.
[a] Each kinetics was analyzed by the proposed method independently in two time windows: (1) from −70 ns to 131 μs and (2) from 80 ns to 131 μs. In every case, the kinetic trace was divided into two equal sequential intervals.
[b] The integral intensity of $^1O_2$ luminescence, I, detected after the photoexcitation of the oxygenated proteins.
[c] The integral intensity of $^1O_2$ luminescence, I_{st}, generated by the photoexcitation of the standard was evaluated by the kinetic method at 1270 nm.

pulses, the dynamics of the photodissociation itself have been under active investigation [33,38,39]. Understanding these primary processes requires a detailed knowledge of the electronic states of this system as well as couplings and interactions between them. A great deal of experimental and theoretical work has been devoted to establish an accurate mapping of the states of various hemoglobin derivatives [40]. Many of the excited states of hemoglobin were experimentally assigned [41], and these results with crystal field calculations [42] were used by Greene et al. [40] to generate a detailed energy level diagram for the oxygenated and deoxygenated hemoglobin. A simplified energy level diagram is shown in Fig. 6. As it is known [39], after photoexcitation into the $^1\pi\pi^*(Q)$ state by 532 nm light, the heme-ligand bond is broken in less than 50 fs. The ratio of the number of photodissociated O_2 molecules to that of absorbed light quanta defines the primary quantum yield of photodissociation, γ_0, being practically the same ($\gamma_0 = 0.23 \pm 0.03$) for oxymyoglobin and oxyhemoglobin [34,43–45]. This value is less than unity primary due to an electronic relaxation to nonreactive low-lying states. After the excitation into the ^1Q state, the oxygenated proteins undergo conventional nonradiative relaxation dynamics. Since spin-allowed processes could be the fastest ones, singlet and triplet states are expected to be reached in the relaxation, charge transfer (CT) states being the lowest ones. Moreover, a second-order spin–orbit interaction allows intersystem crossing from the ^1Q state into the lowest quintet $^5T_2$ state. $^5T_2$ is near the ^1Q state, but not a strong candidate to have significant population soon after pumping ^1Q. Therefore, the spin–orbit interaction influences the initial partitioning of the excitation energy. Although a vast knowledge about the ground and excited states has been accumulated, the precise nature of the excited states involved in their photodissociation processes is still controversial. In principle, the dissociating states may be $\pi\pi^*$ states, as the authors of works [46,47] believe, states of the ligand field (dd states) [38], or charge-transfer states [48].

Fig. 6 also summarizes the energetics for the photochemical dissociation of oxygenated hemoglobin. A 532-nm photon excites the heme into its ^1Q state, thereby depositing 53.8 kcal/mol of energy. The enthalpy difference between $Hb + O_2$ (gas) and HbO_2 is approximately 15.7 kcal/mol (averaged over α and β subunits of hemoglobin) [49], so the heme group and O_2 share approximately 38.1 kcal/mol of excess energy. The partitioning of this excess energy is critically dependent on the mechanism of photodissociation, i.e. which electronic states are involved. A lot of spin-allowed reactions as a source of ground-state molecular oxygen can be proposed [33]. If the excess energy contained in O_2 is more than 22.6 kcal/mol [2,4], then singlet oxygen can be generated. As it is followed from the energy level diagram, only three spin-allowed reactions as a source of singlet oxygen can be proposed:

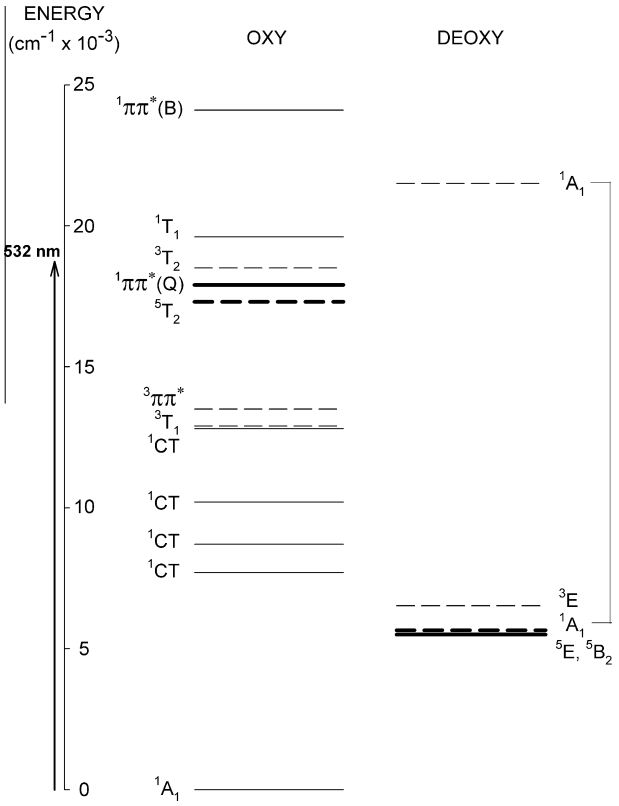

Fig. 6. Simplified energy level diagram (after Greene et al. [40]) for electronic states of the oxygenated and deoxygenated hemoglobin. Energy levels indicated by *solid lines* have been observed in absorption using single crystal, magnetic circular dichroism, and circular dichroism spectroscopy by Eaton et al. [41]. *Dashed lines* indicate approximate energies of levels calculated from crystal field theory. For the oxygenated hemoglobin, the energies in octahedral symmetry are based on $10Dq$ from the $^1A_1 \rightarrow {}^1T_1$ assignment with $C = 4B = 2900\ cm^{-1}$ [41]; for the deoxygenated one, the first-order energies in tetragonal symmetry are based on the orbital splitting [42,50]. The uncertain $^1A_1$ state of deoxy species is drawn both at the crystal field theory position (*ca.* 100 cm^{-1} above the ground state) and at the energy calculated by Olafson and Goddard [18], 16,000 cm^{-1} above the ground state. The $^1\pi\pi^*(Q)$ state is directly excited at 532 nm (18,880 cm^{-1}). The bond energy is approximated by the measured enthalpy change for binding to the gaseous ligand [49]. CT, charge transfer.

$$HbO_2(^1Q) \rightarrow Hb(^1A_1) + O_2(^1\Delta_g), \quad (16)$$

$$HbO_2(^5T_2) \rightarrow Hb(^5E) + O_2(^1\Delta_g), \quad (17)$$

$$HbO_2(^5T_2) \rightarrow Hb(^5B_2) + O_2(^1\Delta_g). \quad (18)$$

In Fig. 6, the mentioned reactant and product states are indicated as *bold lines*. As it is seen, the reactant states are the ^1Q state and the lowest quintet $^5T_2$ state. In the first reaction (Eq. (16)), the expected product state is the lowest excited state, a singlet $^1A_1$. This state is not known from experiment. Some calculations [42,50] place the singlet $^1A_1$ *ca.* 100 cm^{-1} above the ground state, whereas in others [18] the singlet is located 16,000 cm^{-1} above the ground state. In the last case, the dissociation leading to the $^1O_2$ production is improbable. In the last two reactions (Eqs. (17) and (18)), the accessible spin-allowed product is the degenerate quintet ground state (^5E and $^5B_2$) of deoxy-protein. In order to estimate the probability of all the considered dissociation reactions (Eqs. (16)–(18)), a minimal kinetic model for the $^1O_2$ generation during the photodissociation and a subsequent $^1O_2$ deactivation is introduced and discussed in the following Sections. It should be stressed that, in the kinetic model, the photosensitized $^1O_2$ production is neglected since lifetimes of excited-states of the

oxy- and deoxyheme are short enough (no more than a few picoseconds [39]) to preclude an energy transfer in a bimolecular reaction from the excited states of the heme to the ground-state molecular oxygen.

4.2. A minimal kinetic model

After the photodissociation, a certain fraction of ligands rebinds from within the protein matrix. This process is called geminate recombination. In hemoglobin and myoglobin, the geminate O_2 rebinding is completed in less than 0.2 and 1.0 μs, respectively [45,51]. For those proteins from which ligands succeed in escaping into the surrounding medium, rebinding is a bimolecular reaction. With respect to $^1O_2$ emission, the studied protein solutions are nonhomogeneous mediums. In order to describe the time dependence of the $^1O_2$ concentration after the photodissociation, a proper simplified kinetic model (Scheme 1) was introduced. In Scheme 1, the energy level diagram for the $^1O_2$ generation during the photodissociation and a subsequent $^1O_2$ deactivation within the protein and in the surrounding medium are shown schematically. It contains the ground $^1A_1$ state of the oxygenated protein and their reactant ^1Q and $^5T_2$ states. Scheme 1 also contains the ground, $^3O_2$, and first excited singlet state, $^1O_2$, of molecular oxygen, where superscripts "p" and "s" correspond to the molecular oxygen within the protein and in the surrounding medium, respectively. Additionally, the ground states of quenchers and solvent are shown.

After the excitation of oxygenated protein into the ^1Q state, the instantaneous photodissociation occurs which can lead to the $^1O_2$ generation within the protein matrix (Scheme 1, $^1O_2^p$ state). The generated $^1O_2$ can be quenched with amino acids [3] as well as with the heme or can escape completely from the protein matrix into the surrounding medium ($^1O_2^s$ state) [37,45,51]. Subsequently, $^1O_2$ escaped into the solvent can be quenched mainly with water or can return into the protein matrix. Quenching channels including radiative (k_r) and nonradiative (k_{nr}) processes deactivate the excited singlet oxygen both within the proteins (superscript "p") and in the surrounding medium (superscript "s"), the nonradiative processes being dominating [2,4]. Additionally, in the present kinetic model, it is considered that $^1O_2$ can geminately rebind to the heme iron (k_{gem}).

According to Scheme 1, the system of coupled differential equations providing the time dependence of the concentrations of $^1O_2$ within the proteins, $[^1O_2^p](t)$, as well as in the surrounding medium, $[^1O_2^s](t)$, may be set as:

$$\frac{d[^1O_2^p](t)}{dt} = -(k_r^p + k_{nr}^p + k_{gem} + k_{out})[^1O_2^p](t) + k_{in}[P][^1O_2^s](t), \quad (19)$$

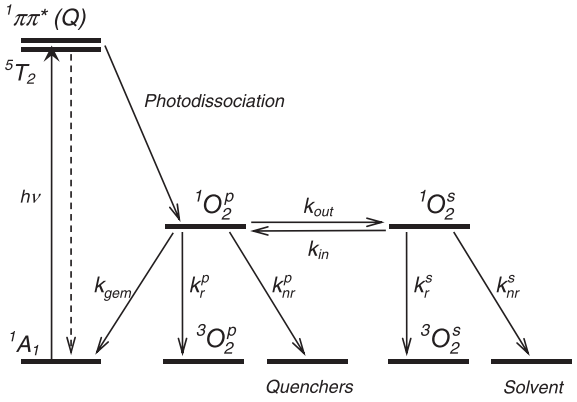

Scheme 1. Reaction scheme for the $^1O_2$ generation during the photodissociation and a subsequent geminate $^1O_2$ rebinding to the heme iron and $^1O_2$ deactivation.

$$\frac{d[^1O_2^s](t)}{dt} = -(k_r^s + k_{nr}^s + k_{in}[P])[^1O_2^s](t) + k_{out}[^1O_2^p](t), \quad (20)$$

where k_r and k_{nr} are the medium-dependent $^1O_2$ radiative and nonradiative rate constants, respectively [52]; k_{gem} is the rate constant for the geminate $^1O_2$ rebinding to the heme iron; k_{out} and k_{in} are the rate constants for $^1O_2$ escape from and entry into the proteins, respectively; $[P]$ is the concentration of proteins in solvent. During the experiment, the protein concentration checked spectroscopically in the visible region was practically constant. Absorbance changes at Q-band maxima do not exceed 1%. It should be noted that the nonradiative constant k_{nr}^p describes both the physical and chemical quenching. The last one results in O_2 consumption. However, due to the low laser energy and continuous stirring at the subsequent laser irradiation, the concentration of O_2 in the working volume can be considered constant. The constancy of O_2 concentration was preliminarily confirmed in experiments where laser flash photolysis technique was used to study bimolecular O_2 rebinding to the proteins under repeating laser irradiation [45,51,53].

In Eqs. (19) and (20), the sum of the medium-dependent $^1O_2$ radiative, k_r, and nonradiative rate constants, k_{nr}, determines the rate constant of $^1O_2$ deactivation within the proteins, k_Δ^p, and in water, k_Δ, respectively:

$$k_\Delta^p = k_r^p + k_{nr}^p, \quad (21)$$

$$k_\Delta = k_r^s + k_{nr}^s. \quad (22)$$

To solve the system of Eqs. (19) and (20), the initial concentration of $^1O_2^p$ state is set equal to $[^1O_2^p]_{t=0}$, while that of $^1O_2^s$ is set 0. Thus, solving the system of differential equations, one can obtain the time dependence of the concentration of $^1O_2$ within the proteins

$$[^1O_2^p](t) = \frac{[^1O_2^p]_{t=0}}{\alpha_1 - \alpha_2}((\alpha_1 - k_\Delta - k_{in}[P])e^{-\alpha_1 t} + (k_\Delta + k_{in}[P] - \alpha_2)e^{-\alpha_2 t}), \quad (23)$$

as well as in the surrounding medium

$$[^1O_2^s](t) = \frac{k_{out}[^1O_2^p]_{t=0}}{\alpha_1 - \alpha_2}(e^{-\alpha_2 t} - e^{-\alpha_1 t}). \quad (24)$$

Here,

$$\alpha_{1,2} = \frac{1}{2}(k_\Delta^p + k_{gem} + k_{out} + k_\Delta + k_{in}[P] \pm \sqrt{(k_\Delta^p + k_{gem} + k_{out} - k_\Delta - k_{in}[P])^2 + 4k_{in}[P]k_{out}}),$$

$$\alpha_1 > \alpha_2. \quad (25)$$

4.3. Quantum yields of singlet oxygen production

The number of $^1O_2$ molecules generated per absorbed photon during the photodissociation of molecular oxygen from the heme defines the primary quantum yield of $^1O_2$ production after the photodissociation, Q_Δ^p:

$$Q_\Delta^p = \frac{[^1O_2^p]_{t=0}}{(N/V)\beta}, \quad (26)$$

where β is the absorption factor of oxygenated proteins at the excitation wavelength. On the other hand, the maximal number of $^1O_2$ molecules generated per absorbed photon during the photodissociation and escaped from the proteins into the surrounding medium defines the quantum yield of $^1O_2$ production in the surrounding medium after the photodissociation, Q_Δ^s:

$$Q_{\Delta}^{s} = \frac{[^1O_2^s]_{t_{max}}}{(N/V)\beta}, \tag{27}$$

where $[^1O_2^s]_{t_{max}}$ is the maximal concentration of $^1O_2$ in the surrounding medium after the photodissociation; t_{max} is the time when the concentration of $^1O_2$ in the surrounding medium, $[^1O_2^s]$ (Eq. (24)), reaches its maximal value, the value of t_{max} being determined as

$$t_{max} = \frac{\ln(\alpha_1/\alpha_2)}{\alpha_1 - \alpha_2}. \tag{28}$$

It should be noted that the ratio $[^1O_2^s]_{t_{max}}/[^1O_2^p]_{t=0}$ represents the efficiency of $^1O_2$ escape from the protein matrix, δ, which is determined as

$$\delta = \frac{k_{out}}{\alpha_1 - \alpha_2}(e^{-\alpha_2 t_{max}} - e^{-\alpha_1 t_{max}}). \tag{29}$$

Additionally, the relationship between the quantum yields Q_{Δ}^{p} and Q_{Δ}^{s} can be obtained:

$$Q_{\Delta}^{s} = Q_{\Delta}^{p}\delta. \tag{30}$$

4.4. Luminescence emitted by photodissociated singlet oxygen

The intensity of luminescence emitted by $^1O_2$ generated during the photodissociation, $S(t)$, is proportional to the concentration of $^1O_2$ both within the proteins and in the surrounding medium:

$$S(t) = \frac{\kappa}{n^2}(k_r^p[^1O_2^p](t) + k_r^s[^1O_2^s](t)). \tag{31}$$

Taking into account the time dependences (23), (24), and (31) one can obtain the integral intensity of luminescence emitted by photodissociated $^1O_2$:

$$I = \frac{\kappa}{n^2}\frac{k_r^p(k_{\Delta} + k_{in}[P]) + k_r^s k_{out}}{(k_{\Delta}^p + k_{gen})(k_{\Delta} + k_{in}[P]) + k_{\Delta}k_{out}}[^1O_2^p]_{t=0}. \tag{32}$$

As it is seen, the integral intensity I is determined by the rate constants for $^1O_2$ radiative deactivation in the proteins, k_r^p, as well as in the surrounding medium, k_r^s. It should be noted that solvent effects on the radiative rate constant k_r have been the subject of intense experimental investigations [54,55]. A correlation between k_r and the solvent refractive index n has been observed [55]. Based on the known relationship between k_r and n [55], and taking the refractive indexes for the proteins and surrounding medium (water buffer) to be equal to 1.6 [56] and 1.333, respectively, one can estimate the ratio between the radiative rate constant for $^1O_2$ deactivation within the proteins and the one in the surrounding medium: $\xi = k_r^p/k_r^s$. The parameter ξ was estimated to be equal to 10. Finally, using Eqs. (32) and (26), the integral intensity I can be expressed in terms of the primary quantum yield of $^1O_2$ production, Q_{Δ}^{p}:

$$I = Q_{\Delta}^{p}\frac{\kappa k_r^s}{n^2}\frac{\xi(k_{\Delta} + k_{in}[P]) + k_{out}}{(k_{\Delta}^p + k_{gem})(k_{\Delta} + k_{in}[P]) + k_{\Delta}k_{out}}(N/V)\beta. \tag{33}$$

4.5. A comparative method for quantum yield determination

The integral intensity of $^1O_2$ luminescence, I (Eq. (33)), can be compared with the one emitted by $^1O_2$ generated by the photosensitizer, I_{st} (Eq. (8)). In such a comparison, the parameters κ, N, and V are canceled since all the samples are excited under the same geometrical conditions with the same laser energy. Additionally, the parameter n is canceled as well since the experimentally measured refractive indexes of the standard and protein solutions are practically the same. Thus, using Eqs. (33) and (8), the primary quantum yield of $^1O_2$ production after the photodissociation, Q_{Δ}^{p}, can be obtained:

$$Q_{\Delta}^{p} = Q_{\Delta}^{st}\frac{I}{I_{st}}\frac{\beta_{st}}{\beta}\frac{(k_{\Delta}^p + k_{gem})(k_{\Delta} + k_{in}[P]) + k_{\Delta}k_{out}}{\xi k_{\Delta}(k_{\Delta} + k_{in}[P]) + k_{\Delta}k_{out}}. \tag{34}$$

Obviously, the number of $^1O_2$ molecules generated during the photodissociation is less or equal to the number of photodissociated O_2 molecules. Consequently, the following constraint is valid:

$$Q_{\Delta}^{p} \leqslant \gamma_0. \tag{35}$$

This is the rationale for the comparative method for determination of the primary quantum yield Q_{Δ}^{p} in terms of the experimentally measured parameters.

4.6. Upper limits for the quantum yields of singlet oxygen production

In the present work, the time-resolved luminescence measurements in the near-infrared region indicated that the photodissociation of molecular oxygen from myoglobin and hemoglobin does not produce detectable quantities of singlet oxygen. The simple and highly sensitive method of luminescence quantification was developed and used to determine the upper limit for the integral intensity I (Table 2). Subsequently, the upper limit for I was used to find the upper limit for the primary quantum yield of $^1O_2$ production after the photodissociation, Q_{Δ}^{p}, by applying Eq. (34) at the constraint (35). Moreover, the upper limit for I was also used to find the upper limit for the quantum yield of $^1O_2$ production in the surrounding medium after the photodissociation, Q_{Δ}^{s}, by applying Eqs. (30) and (34).

To estimate the quantum yields Q_{Δ}^{p} and Q_{Δ}^{s}, the rate constants for $^1O_2$ entry into and escape from the proteins were taken to be equal to $k_{in} = 3.7 \times 10^7\ M^{-1}s^{-1}$ and $k_{out} = 7.6 \times 10^6\ s^{-1}$, respectively, being obtained using published results of laser flash-photolysis studies of O_2 rebinding to myoglobin [45]. A key role in the O_2 rebinding is played by protein cavities that describe paths between the surrounding medium and the heme iron. In the present work, the rate constants k_{in} and k_{out} for hemoglobin were taken to be equal to those for myoglobin, suggesting similar migration processes for both considered proteins. Moreover, the migration routes of molecular oxygen in both the ground triplet state and the singlet excited state are considered the same. It should be stressed that the rate constant for $^1O_2$ entry into the proteins, k_{in}, can be taken to be equal to rate constants for oxygen quenching of excited triplet states of fluorescent porphyrins in substituted myoglobin and hemoglobin, commonly used to measure O_2 diffusion from the ambient solution through the protein to the heme pocket [57,58]. If the rate constant k_{in} were taken to be equal to the quenching rate constant being varied from $9.6 \times 10^7\ M^{-1}\ s^{-1}$ [57] to $1.8 \times 10^8\ M^{-1}\ s^{-1}$ [58], the under-mentioned estimates of quantum yields Q_{Δ}^{p} and Q_{Δ}^{s} do not change. The rate constant of $^1O_2$ deactivation in the surrounding medium, k_{Δ}, was found in an additional flash photolysis experiment (setup as in Ref. [51]) to be equal to $(2.78 \pm 0.15) \times 10^5\ s^{-1}$. The rate constant k_{Δ} measured by us agree well with those reported previously [4,26,29–32]. Unfortunately, the rate constant for the geminate $^1O_2$ rebinding to the heme iron, k_{gem}, and the rate constant of $^1O_2$ deactivation within the proteins, k_{Δ}^{p}, which are crucial for the estimates of Q_{Δ}^{p} as well as Q_{Δ}^{s}, are unknown. However, it can be expected that the rate constant k_{Δ}^{p} depends significantly on $^1O_2$ quenchers in the distal heme pocket where singlet oxygen would be generated. The distal heme pocket is bounded by the heme and a number of hydrophobic amino acids. The most important one is the distal histidine, HisE7, being a probable candidate for $^1O_2$ quencher. Bimolecular rate constants for the quenching of $^1O_2$ with solvated iron-porphyrins and histidine are known to be equal to $\sim 1 \times 10^9$ - $M^{-1}\ s^{-1}$ [59] and $\sim 5 \times 10^7\ M^{-1}\ s^{-1}$ [60], respectively. However, little is known about rate constants for reactions between $^1O_2$ and the quenchers when the latter are in a protein. The rate constants

for $^1O_2$ reaction with amino acids depend significantly on the position of these quenchers in a given protein [61]. A local protein environment can either inhibit or accelerate the $^1O_2$ quenching appreciably by perturbing the electronic distribution in amino acids and increasing the local viscosity [61]. At present, it is difficult to predict the rate constants for reactions between $^1O_2$ and the quenchers when the latter are in the studied proteins. Nevertheless, taking into account that the bimolecular rate constant for the $^1O_2$ quenching by solvated iron-porphyrins [59] is about 20 times larger than the one for the $^1O_2$ quenching by solvated histidine [60], we speculate that, within the distal heme pocket, $^1O_2$ is mainly quenched by the heme. This quenching proceeds through a collisional complex between $^1O_2$ and the heme. It was suggested previously [59] that $^1O_2$ quenching by solvated iron-porphyrins is mediated by charge transfer at the heme iron center. Taking this into consideration, it is expected that the complex between $^1O_2$ and the heme within the proteins contains an appreciable charge transfer character. When there is a good coupling between electronic states (i.e., ground, charge transfer, and locally excited states) of the collisional complex, any formed singlet oxygen can be rapidly deactivated [62]. It should be stressed that, immediately after the photodissociation, singlet oxygen would be in the close vicinity to the heme that might result in an efficient $^1O_2$ quenching. Previously [63], it was shown that the bimolecular rate constant of physical quenching of singlet oxygen by solvated iron-porphyrins is more than five orders in magnitude larger than the bimolecular rate constant of chemical quenching. Thus, we speculate that $^1O_2$ deactivation by the heme within the proteins proceeds through an intermediate with appreciable charge transfer character, the physical deactivation channel being dominating. It should be noted that the ability of the heme to deactivate $^1O_2$ physically is important for normal hemoglobin and myoglobin functions (molecular oxygen transport and storage, respectively).

In spite of all the above-mentioned speculations, we do not know the exact values of the rate constant of $^1O_2$ deactivation within the proteins, k_Δ^p, and the rate constant for the geminate $^1O_2$ rebinding to the heme iron, k_{gem}. To overcome these difficulties, the estimates of the quantum yields Q_Δ^p and Q_Δ^s are performed as a function of the sum of the rate constants k_Δ^p and k_{gem}. The sum is varied from 0 s^{-1} up to the maximum permissible level of 10^{12} s^{-1}. The obtained dependence of the upper limit for the primary quantum yield of $^1O_2$ production after the photodissociation, Q_Δ^p (Eq. (34)), on the sum of the rate constants k_Δ^p and k_{gem} for myoglobin is shown in Fig. 7 (*solid curve*). For comparison, the value of the primary quantum yield of photodissociation, γ_0, is presented as *open circles*. Additionally, the decision region for Q_Δ^p is shown as *gray area*. As it is seen, at the sum $k_\Delta^p + k_{gem}$ smaller than 10^5 s^{-1}, the upper limit for Q_Δ^p approaches its minimal value of 2×10^{-3}, being two orders of magnitude smaller than γ_0. This means that, on the average, no more than one from every hundred photodissociated molecules can be in the excited singlet state. At the sum $k_\Delta^p + k_{gem}$ larger than 8×10^8 s^{-1}, the upper limit for Q_Δ^p approaches its maximal value, which is equal to that of the primary quantum yield of photodissociation, γ_0. This means that all photodissociated oxygen molecules can be in the excited singlet state. However, because of the highly efficient $^1O_2$ quenching and fast geminate $^1O_2$ rebinding, the excited molecules do not emit photons in amount large enough to be detectable. The obtained dependence of the upper limit for the quantum yield of $^1O_2$ production in the surrounding medium after the photodissociation, Q_Δ^s, on the sum $k_\Delta^p + k_{gem}$ for myoglobin is also shown in Fig. 7 (*dashed curve*). The decision region for Q_Δ^s is below the corresponding line. Obviously, the quantum yield Q_Δ^s cannot be larger than the primary quantum yield Q_Δ^p. As it is seen, at all possible values of the sum $k_\Delta^p + k_{gem}$, the upper limit for Q_Δ^s does not exceed 2.3×10^{-3}.

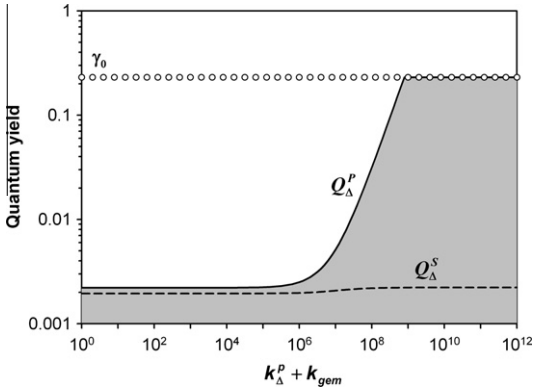

Fig. 7. Dependencies of the upper limits for the primary quantum yield of $^1O_2$ production after the photodissociation, Q_Δ^p, and the quantum yield of $^1O_2$ production in the surrounding medium after the photodissociation, Q_Δ^s, on the sum of the rate constant of $^1O_2$ deactivation within the proteins, k_Δ^p, and the rate constant for the geminate $^1O_2$ rebinding to the heme iron, k_{gem}. The dependencies of Q_Δ^p and Q_Δ^s for myoglobin are shown by *solid* and *dashed curves*, respectively. The decision region for Q_Δ^p is shown as *gray area*. For comparison, the value of the primary quantum yield of photodissociation, γ_0, is presented as *open circles*.

Similarly, the values of Q_Δ^p and Q_Δ^s for oxyhemoglobin were estimated. The dependences of Q_Δ^p and Q_Δ^s for oxyhemoglobin are similar with those for oxymyoglobin (not shown). The upper limit for Q_Δ^s does not exceed 3.4×10^{-3}. Thus, the estimated quantum yields of $^1O_2$ production in the surrounding medium after the photodissociation, Q_Δ^s, for oxyhemoglobin and oxymyoglobin are at least 68 and 105-times, respectively, smaller than the primary quantum yields of photodissociation, γ_0. This means that, on the average, no more than one molecule of singlet oxygen from every hundred photodissociated oxygen molecules can succeed in escaping from the protein matrix of myoglobin as well as hemoglobin.

5. Conclusions

In the present work, the time-resolved luminescence measurements in the near-infrared region indicated that photodissociation of molecular oxygen from myoglobin and hemoglobin does not produce detectable quantities of singlet oxygen. The simple and highly sensitive method of luminescence quantification was developed and used to determine the upper limits for the quantum yields of singlet oxygen production. The proposed method was preliminary evaluated using model data sets and confirmed with experimental data for porphyrin solutions. The method was shown to provide a determination of the integral luminescence intensity in a wide range of values even for kinetics with extremely low signal-to-noise ratio.

The present experimental data, obtained with the state-of-the-art technique, do not deny the possibility of singlet oxygen generation during the photodissociation of molecular oxygen from myoglobin and hemoglobin, and, consequently, the possibilities of all the considered dissociation reactions (Eqs. (16)–(18)). It is speculated that within the distal heme pocket, singlet oxygen is mainly quenched by the heme. Moreover, the singlet oxygen deactivation by the heme is suggested to proceed through a collisional complex with appreciable charge transfer character, the physical deactivation channel being dominating. The photodissociation of molecular oxygen from myoglobin and hemoglobin was found to be not efficient to yield singlet oxygen escaped from the proteins into the surrounding medium. On the average, no more than one molecule of singlet oxygen from every hundred photodissociated oxygen molecules can succeed in escaping from the protein matrix.

6. Abbreviations

CT	charge transfer
Hb	hemoglobin
HbO_2	oxyhemoglobin
Mb	myoglobin
MbO_2	oxymyoglobin
NIR	near-infrared region
$O_2(^1\Delta_g)$ or $^1O_2$	singlet oxygen
O_2	molecular oxygen
PMT	photomultiplier tube
TMPyP	5,10,15,20-tetrakis(4-*N*-methylpyridyl) porphyrin

Acknowledgments

This work was supported by the Foundation of Basic Research of the Republic of Belarus (Grant No. Ph11Y-084) and by the National Academy of Sciences of Belarus through the Program "Electronics and photonics" (Project 2.3.03).

References

[1] V.R.I. Kaila, M.I. Verkhovsky, M. Wikström, Proton-coupled electron transfer in cytochrome oxidase, Chem. Rev. 110 (2010) 7062–7081.
[2] A.A. Krasnovsky Jr., Luminescence and photochemical studies of singlet oxygen photonics, J. Photochem. Photobiol. A: Chem. 196 (2008) 210–218.
[3] C.S. Foote, in: W.A. Pryor (Ed.), Free Radicals in Biology, vol. 2, Academic Press, New York, 1976.
[4] C. Schweitzer, R. Schmidt, Physical mechanisms of generation and deactivation of singlet oxygen, Chem. Rev. 103 (2003) 1685–1757.
[5] B.F. Minaev, Electronic mechanisms of molecular oxygen activation, Russ. Chem. Rev. 76 (2007) 988–1010.
[6] D.M. Wagnerová, K. Lang, Photorelease of triplet and singlet oxygen from dioxygen complexes, Coord. Chem. Rev. 255 (2011) 2904–2911.
[7] P.R. Ogilby, Singlet oxygen: there is still something new under the sun, and it is better than ever, Photochem. Photobiol. Sci. 9 (2010) 1543–1560.
[8] A.N. Macpherson, A. Telfer, J. Barber, T.G. Truscott, Direct detection of singlet oxygen from isolated Photosystem II reaction centres, Biochim. Biophys. Acta 1143 (1993) 301–309.
[9] A.U. Khan, P. Gebauer, L.P. Hager, Chloroperoxidase generation of singlet Δ molecular oxygen observed directly by spectroscopy in the 1- to 1.6-μm region, Proc. Natl. Acad. Sci. USA 80 (1983) 5195–5197.
[10] J.R. Kanofsky, Singlet oxygen production by lactoperoxidase. Evidence from 1270 nm chemiluminescence, J. Biol. Chem. 258 (1983) 5991–5993.
[11] J.R. Kanofsky, B. Axelrod, Singlet oxygen production by soybean lipoxygenase isozymes, J. Biol. Chem. 261 (1986) 1099–1104.
[12] J.R. Kanofsky, Singlet oxygen production by bleomycin: a comparison with heme-containing compounds, J. Biol. Chem. 261 (1986) 13546–13550.
[13] J.R. Kanofsky, H. Hoogland, R. Wever, S.J. Weiss, Singlet oxygen production by human eosinophils, J. Biol. Chem. 263 (1988) 9692–9696.
[14] A.U. Khan, M. Kasha, Singlet molecular oxygen in the Haber-Weiss reaction, Proc. Natl. Acad. Sci. USA 91 (1994) 12365–12367.
[15] R.W. Redmond, I.E. Kochevar, Spatially resolved cellular responses to singlet oxygen, Photochem. Photobiol. 82 (2006) 1178–1186.
[16] D.A. Case, B.H. Huynh, M. Karplus, Binding of oxygen and carbon monoxide to hemoglobin. An analysis of the ground and excited states, J. Am. Chem. Soc. 101 (1979) 4433–4453.
[17] K.P. Jensen, U. Ryde, How O_2 binds to heme: reasons for rapid binding and spin inversion, J. Biol. Chem. 279 (2004) 14561–14569.
[18] B.D. Olafson, W.A. Goddard III, Molecular description of dioxygen bonding in hemoglobin, Proc. Natl. Acad. Sci. USA 74 (1977) 1315–1319.
[19] W.A. Goddard, B.D. Olafson III, Ozone model for bonding of an O_2 to heme in oxyhemoglobin, Proc. Natl. Acad. Sci. USA 72 (1975) 2335–2339.
[20] J.J. Weiss, Nature of the iron-oxygen bond in oxyhæmoglobin, Nature 202 (1964) 83–84.
[21] L. Pauling, Nature of the iron-oxygen bond in oxyhæmoglobin, Nature 203 (1964) 182–183.
[22] T.E. Tsai, J.L. Groves, C.S. Wu, Electronic structure of iron-dioxygen bond in oxy-Hb-A and its isolated oxy - α and oxy-β chains, J. Chem. Phys. 74 (1981) 4306–4314.
[23] E. Bucci, C. Fronticelli, A new method for the preparation of α and β subunits of human hemoglobin, J. Biol. Chem. 240 (1965) 551–552.
[24] V.A. Galievsky, A.S. Stasheuski, V.V. Kiselyov, A.I. Shabusov, M.V. Belkov, B.M. Dzhagarov, Laser NIR lifetime spectrometer with nanosecond time resolution, Instrum. Exp. Tech. 53 (2010) 568–574.
[25] J.B. Verlhac, A. Gaudemer, I. Krajlic, Water-soluble porphyrins and metalloporphyrins as photosensitizers in aerated aqueous solutions. I. Detection and determination of quantum yield of formation of singlet oxygen, Nouv. J. Chim. 8 (1984) 401–406.
[26] P.K. Frederiksen, S.P. McIlroy, C.B. Nielsen, L. Nikolajsen, E. Skovsen, M. Jørgensen, K.V. Mikkelsen, P.R. Ogilby, Two-photon photosensitized production of singlet oxygen in water, J. Am. Chem. Soc. 127 (2005) 255–269.
[27] S. Nonell, S.E. Braslavsky, Time-resolved singlet oxygen detection, Method Enzymol. 319 (2000) 37–49.
[28] J. Baier, T. Fuβ, C. Pöllmann, C. Wiesmann, K. Pindl, R. Engl, D. Baumer, M. Maier, M. Landthaler, W. Bäumler, Theoretical and experimental analysis of the luminescence signal of singlet oxygen for different photosensitizers, J. Photochem. Photobiol. B: Biol. 87 (2007) 163–173.
[29] S.Yu. Yegorov, A.A. Krasnovskii Jr., Photosensitized luminescence of oxygen on pulsed laser excitation. Kinetics of decay in aqueous solutions, Biophysics 28 (1983) 532–534.
[30] M.A.J. Rodgers, P.T. Snowden, Lifetime of $O_2(^1\Delta_g)$ in liquid water as determined by time-resolved infrared luminescence measurements, J. Am. Chem. Soc. 104 (1982) 5541–5543.
[31] K.I. Salokhiddinov, B.M. Dzhagarov, G.D. Egorova, Direct lifetime measurement of molecular oxygen in singlet $^1\Delta_g$ state generated in water by porphyrin-sensitizer, Opt. Spektr. 55 (1983) 71–73.
[32] F. Wilkinson, W.P. Helman, A.B. Ross, Rate constants for the decay and reactions of the lowest electronically excited singlet state of molecular oxygen in solution. An expanded and revised compilation, J. Phys. Chem. Ref. Data 24 (1995) 663–1021.
[33] B.M. Dzhagarov, V.S. Chirvony, G.P. Gurinovich, Picosecond dynamics of electronic excitation energy redistribution in metalloporphyrins, in: V.S. Letokhov (Ed.), Laser Picoseconds Spectroscopy and Photochemistry of Biomolecules, Adam Hilger, Bristol, 1987, pp. 137–182.
[34] S.V. Lepeshkevich, J. Karpiuk, I.V. Sazanovich, B.M. Dzhagarov, A kinetic description of dioxygen motion within alpha- and beta-subunits of human hemoglobin in the R-state: geminate and bimolecular stages of the oxygenation reaction, Biochemistry 43 (2004) 1675–1684.
[35] S. Sottini, S. Abbruzzetti, C. Viapiani, S. Bettati, L. Ronda, A. Mozzarelli, Evidence for two geminate rebinding states following laser photolysis of R state hemoglobin encapsulated in wet silica gels, J. Phys. Chem. B 109 (2005) 11411–11413.
[36] J. Huang, A. Ridsdale, J. Wang, J.M. Friedman, Kinetic hole burning, hole filling, and conformational relaxation in heme proteins: direct evidence for the functional significance of a hierarchy of dynamical processes, Biochemistry 36 (1997) 14353–14365.
[37] S.V. Lepeshkevich, S.A. Biziuk, A.M. Lemeza, B.M. Dzhagarov, The kinetics of molecular oxygen migration in the isolated α chains of human hemoglobin as revealed by molecular dynamics simulations and laser kinetic spectroscopy, Biochim. Biophys. Acta 1814 (2011) 1279–1288.
[38] D.A. Chernoff, R.M. Hochstrasser, A.W. Steele, Geminate recombination of O_2 and hemoglobin, Proc. Nat. Acad. Sci. USA 77 (1980) 5606–5610.
[39] J.W. Petrich, C. Poyart, J.L. Martin, Photophysics and reactivity of heme proteins: a femtosecond absorption study of hemoglobin, myoglobin, and protoheme, Biochemistry 27 (1988) 4049–4060.
[40] B.I. Greene, R.M. Hochstrasser, R.B. Weisman, W.A. Eaton, Spectroscopic studies of oxy- and carbonmonoxyhemoglobin after pulsed optical excitation, Proc. Natl. Acad. Sci. USA 75 (1978) 5255–5259.
[41] W.A. Eaton, L.K. Hanson, P.J. Stephens, J.C. Sutherland, J.B.R. Dunn, Optical spectra of oxy- and deoxyhemoglobin, J. Am. Chem. Soc. 100 (1978) 4991–5003.
[42] H. Eicher, D. Bade, F. Parak, Theoretical determination of the electronic structure and the spatial arrangement of ferrous iron in deoxygenated sperm whale myoglobin and human hemoglobin from Mössbauer experiments, J. Chem. Phys. 64 (1976) 1446–1455.
[43] B.M. Dzhagarov, V.A. Galievsky, N.N. Kruk, M.D. Yakutovich, Photodissociation of oxygenated forms of the native hemoglobin HbA and its isolated α-and β-subunits and kinetics of molecular oxygen rebinding, Dokl. Biophys. (Doklady Akademii Nauk) 366 (1999) 38–41.
[44] X. Ye, A. Demidov, P.M. Champion, Measurements of the photodissociation quantum yields of MbNO and MbO_2 and the vibrational relaxation of the sixcoordinate heme species, J. Am. Chem. Soc. 124 (2002) 5914–5924.
[45] S.V. Lepeshkevich, B.M. Dzhagarov, Effect of zinc and cadmium ions on structure and function of myoglobin, Biochim. Biophys. Acta 1794 (2009) 103–109.
[46] B.M. Hoffman, Q.H. Gibson, On the photosensitivity of liganded hemoproteins and their metal – substituted analogues, Proc. Natl. Acad. Sci. USA 75 (1978) 21–25.
[47] B.M. Dzhagarov, N.N. Kruk, S.A. Tikhomirov, V. Gulbinas, G.M. Andreyuk, Laser picosecond and nanosecond flash-photolysis of hemoglobin: excited-state spectra and lifetimes, oxygen photodissociation and recombination, the pH-effect, Lietuvos fizikos žurnalas 34 (1994) 108–113.
[48] A. Waleh, G.H. Loew, Quantum mechanical studies of the photodissociation of oxyheme complexes, J. Am. Chem. Soc. 104 (1982) 2352–2356.
[49] F.C. Mills, G.K. Ackers, H.T. Gaud, S.J. Gill, Thermodynamic studies on ligand binding and subunit association of human hemoglobins. Enthalpies of binding O_2 and CO to subunit chains of hemoglobin A, J. Biol. Chem. 254 (1979) 2875–2880.
[50] B.H. Huynh, G.C. Papaefthymiou, C.S. Yen, J.L. Groves, C.S. Wu, Electronic structure of Fe^{2+} in normal human hemoglobin and its isolated subunits, J. Chem. Phys. 61 (1974) 3750–3758.

[51] S.V. Lepeshkevich, M.V. Parkhats, I.I. Stepuro, B.M. Dzhagarov, Molecular oxygen binding with α and β subunits within the R quaternary state of human hemoglobin in solutions and porous sol–gel matrices, Biochim. Biophys. Acta 1794 (2009) 1823–1830.
[52] D. Mogilevtsev, A. Maloshtan, S.V. Lepeshkevich, B.M. Dzhagarov, Spontaneous emission of singlet oxygen near dielectric nano-objects and radiative diagnostics of bio-objects, J. Fluoresc. 22 (2012) 1415–1419.
[53] S.V. Lepeshkevich, B.M. Dzhagarov, Mutual effects of proton and sodium chloride on oxygenation of liganded human hemoglobin: oxygen affinities of the α and β subunits, FEBS J. 272 (2005) 6109–6119.
[54] R.D. Scurlock, P.R. Ogilby, Effect of solvent on the rate constant for the radiative deactivation of singlet molecular oxygen ($^1\Delta_g O_2$), J. Phys. Chem. 91 (1987) 4599–4602.
[55] R.D. Scurlock, S. Nonell, S.E. Braslavsky, P.R. Ogilby, Effect of solvent on the radiative decay of singlet molecular oxygen ($a^1\Delta_g$), J. Phys. Chem. 99 (1995) 3521–3526.
[56] J. Babul, E. Stellwagen, Measurement of protein concentration with interferences optics, Anal. Biochem. 28 (1969) 216–221.
[57] N. Barboy, J. Feitelson, Quenching of the zinc-protoporphyrin triplet state as a measure of small-molecule diffusion through the structure of myoglobin, Biochemistry 26 (1987) 3240–3244.
[58] B. Alpert, L. Lindqvist, Porphyrin triplet state probing the diffusion of oxygen in hemoglobin, Science 187 (1975) 836–837.
[59] E.A. Venediktov, A.A. Krasnovsky Jr., Quenching of luminescence of singlet molecular oxygen by porphyrin complexes with high-charge metal ions, Biophysics 25 (1980) 347–348.
[60] A. Michaeli, J. Feitelson, Reactivity of singlet oxygen toward amino acids and peptides, Photochem. Photobiol. 59 (1994) 284–289.
[61] R.L. Jensen, J. Arnbjerg, P.R. Ogilby, Reaction of singlet oxygen with tryptophan in proteins: a pronounced effect of the local environment on the reaction rate, J. Am. Chem. Sci. 134 (2012) 9820–9826.
[62] M. Kristiansen, R.D. Scurlock, K.-K. Iu, P.R. Ogilby, Charge-transfer state and singlet oxygen ($^1\Delta_g$ O_2) production in photoexcited organic molecule-molecular oxygen complexes, J. Phys. Chem. 95 (1991) 5190–5197.
[63] A.A. Krasnovsky Jr., E.A. Venediktov, O.M. Chernenko, Quenching of singlet oxygen by the chlorophylls and porphyrines, Biophysics 27 (1982) 1009–1016.